ISSN: 2754-4753

Journal of Physics & Optics Sciences

SCIENTIFIC Research and Community

Review Article

Open Access

New Manifestations of the Strong Nuclear Interactions in Solids

Plekhanov VG

Fonoriton Sci. Lab., Garon LtD, 11413, Tallinn, Estonia

ABSTRACT

The discovery of global macroscopic, including optical, characteristics with the addition of one neutron made crystals LiH, LiD, Diamond, Graphene an excellent model for studying the strong nuclear interaction. New manifestations of strong interaction in solids are measurements of its dependence on the distance between nucleons, finding a neutron - electron binding energy (106 meV), which is in excellent agreement with the prediction of the theory (106,7 meV). Moreover, the creation of mass in massless Dirac fermions in graphene by strong nuclear interaction has been demonstrated for the first time.

***Corresponding author**

Plekhanov VG, Fonoriton Sci. Lab., Garon LtD, 11413, Tallinn, Estonia.

Received: April 02, 2024; **Accepted:** April 22, 2024; **Published:** May 10, 2024

Keywords: Strong Interaction, Quarks, Gluons, Excitons, Phonons, QED, QCD

Introduction

Poor understanding of the origin strong nuclear interaction challenges the applications of various methods of its research. Classical low - temperature optic solid-state spectroscopy has received a new revival in the study of the nature of nuclear physics. Precision spectroscopy has long standing record of providing insights into fundamental physics. The hydrogen atom has a central position in the history of the 20th - century physics. Simple atoms, like hydrogen, being essentially quantum electrodynamics (QED) systems, allow highly accurate theoretical predictions. QED is the first successful and still the most successful quantum field theory. The spectacular success of QED gives physicists great confidence in Maxwell's equation on the one hand and Dirac's equation on the other, yet something is missing in relations between them (see, e.g. [2]). After the discovery of the neutron in 1932 by Chadwick [3], there was no longer doubt that the building block of nuclei are proton and neutron (collectively called nucleons) [4]. The discovery of the neutron may be viewed as the birth of the strong nuclear interaction [5, 6]: it indicated that the nuclei consist of protons and neutrons and hence the presence of a force that holds them together, strong enough to counteract the electromagnetic repulsion. A common place in modern physics is the short range of a strong nuclear interaction - the heart of Quantum Chromodynamics, which is part of the Standard Model (SM) [7]. According to SM the strong forces does not act on leptons (electrons, positrons, muons, neutrinos), but only on protons and neutrons. The lack of experimental evidence for this strong statement is tacitly perceived as the only correct (see, e.g. [8]).

Atomic and nuclear physics are two flourishing but distinct branches of physics, the subject of isotope shifts in atomic spectra is one of the few that links these two branches. The successful study of the change in macroscopic characteristics of a solid, on the example of unique crystals LiH and LiD, the addition of one neutron stimulates the study of global changes in macroscopic characteristics of carbon allotropes (diamond, graphite, graphene). The expansion of the studied objects allows not only verify the correctness of the previously obtained results, but also to formulate a new one, which is integral to the development of models of understanding physics (see also [9]).

The phenomenological basis for strong nuclear interaction was laid down by Yukawa's paper [10]. Yukawa's potential has the form

$$V = g\frac{e^{-kr}}{r^n} \qquad (1)$$

for some n. Here the strength of the force is measured by the constant k (see, also [5]). The most important feature Yukawa's forces are that they have a small range (~10^{-15} m). The central dogma of atomic physics after Yukawa's paper that proton - electron attraction could be explained in terms of classical electrostatic theory, while the strong force effects were essentially new and inexplicable. So, far the best theoretical guess is the Yukawa potential, but it is a static potential not dependent on velocities of the nucleons. A static force is not a complete one because it cannot explain the propagation of the nuclear interaction. Moreover, as was indicated above, a phenomenological Yukawa potential cannot be directly verified experimentally. We should note that nowadays in text books and elsewhere the separation of electromagnetic and strong interaction tacitly assumed. It is very strange up to present time we do not even know the strong force very well. And what is more we having some contradiction taking into account that the forces between quarks must be long - range, because the gluons have zero mass. But as was mentioned above the force between colorless hadrons is short - range, when the distance between hadrons is more than nuclear size [8].

As indicated above, there is a common place in Standard Model (SM) of modern physics that the strong force does not act on leptons (see, also [7]). Following this conclusion we do not must to observe the dependence of the optical properties of solids on addition neutrons in substance. This contradicts the history of the development of isotope effect. The first attempt to discover an

interaction between neutrons and electrons was made by Dee [11] in the same year, 1932 in which the neutron was discovered by Chadwick [3]. In 1936, Condon [12] pointed out that the existence of a neutron - electron interaction would give rise to an isotope shift in spectral lines of atoms, which was observed for the first time by Aronberg in 1918 [13] in the line spectra of Pb isotopes (see, also [14, 15]). The existence of a weak attractive interaction between electrons and neutrons has been described in the series papers by Foldy [16]. Foldy has showed that neutron - electron interaction has two contributions - one arising from anomalous magnetic moment of the neutron (see, also [5]) and the other from an intrinsic Darwin coefficient [17] - electric field. This picture was justifiable in meson theory though both of these contributions have a common origin [12, 16]. In all methods of the measurements (see, e.g. [16]) there are principal troubles connected with the necessity of introducing large corrections in size of order of the investigated effect of neutron - electron interaction. Besides there is intrigue in the fact that all known experimental values (see [19] and references quoted therein) were scattered around the so called Foldy scattering length in the interval ±10%. The main conclusion of the fundamental papers by Foldy is that the intrinsic neutron - electron interaction is essentially an electromagnetic interaction between the neutron and the charge density producing an external electromagnetic field by electron [16, 19]. We add that the present paper on the mass isotopic effect (light isotopes) is the first among the works [20 - 25] engaged in the search for new physics (and the origin of mass) studying the isotopic effect caused by a change in volume (interaction with the environment of isotopes with large mass) (see also [26]). We emphasize that in these works the main thing is the search for new physics abroad of the SM, the core of which is the search and measurement of neutron - electron interaction, as in our previously published articles [27-30].

Experimental Results and Discussion

Before beginning a general discussion of new manifestations of the strong nuclear interaction, it is helpful to have an idea of electronic structure of bulk materials. As is well - known the nature of materials is determined by the interaction of their valence electrons with their charged nuclei and core electrons. This determines how elements react with each other, what structure the solid prefers, its optoelectronic properties and all other aspects of the material. The modern view of solid-state physics is based on the presentation of elementary excitations, having mass, quasiimpuls, electrical charge and so on [31]. According to this presentation the elementary excitations of the non - metallic materials are electrons (holes), excitons (polaritons) and phonons. The theory discussed in modern text books (see, e.g. [32]) forms the basis for the modern theory of electrons in solid. It arises from the consideration of the periodicity of the crystal structure. This periodicity leads to the formation of energy bands (see Figure 1). The importance of the electronic theory of solids as embodied in band theory is that it provides us with clear means of understanding how solids may be insulators, semiconductors, or metals. This depends upon whether or not it is Fermi surface. The existence of a Fermi surface produces metallic behavior, whereas at 0K, if the filled electron levels (bands in solids - see Figure 1) are separated from vacant ones, we have insulating properties. The difference between a good conductor and a good insulator is striking. The electrical resistivity of a pure metal may be as low as 10^{-10} ohm-cm at a temperature of 1 K, apart from the possibility of superconductivity. The resistivity of good insulator may as high as 10^{22} ohm-cm. The understand the difference between insulators and conductors, we shall use the band – gap picture (Figure 1). The possibility of band gap is the most important property of solids.

In crystals allowed electron energies typically have an energy band structure that may be understood as follows. If two atoms, each with the same energy, come close to each other, the composite two - atom system is characterized by two close energy levels. Similarly, for a system of N atoms, every energy level of the isolate atom is split into N closely space levels. This assembly of close levels may be considered as an energy band (see more below Figure 5). A crucial point is the filling of the bands by electrons. under equilibrium conditions and at low ambient temperature, the lowest energy levels should be populated. The most important electrons are those in the upper populated bands. All bands are completely filled are separated from the upper (empty) bands by the energy gap E_g (Figure 1). For insulators the band gap is $E_g \geq 5$eV, for semiconductors is $E_g \leq 5$ eV. To better understand the difference between insulators and conductors, we must extend the free electron model [32] to take into account of the periodic lattice of the solid. The possibility of a band gap is the most important new property than emerges.

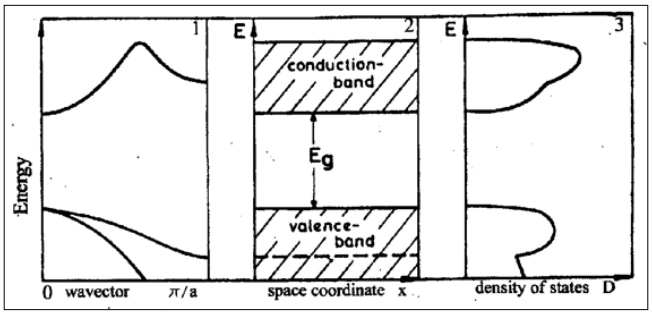

Figure 1: Various possibilities to present the band - structure of homogeneous undoped insulator (semiconductor). 1 - the dispersion relation, i.e. the energy E as a function of the wave vector $\bar{k}$, 2 - the energy regions of allowed and forbidden states as function of a space coordinate x and 3 - the density of states (all curves are schematic ones)

According to modern concept, the excitons can be considered [33] as the excited of the N - particles system: An electron from the valence band (see Figure 1) is excited into the conduction band. The attractive Coulomb potential between the missing electron in the valence band, which can be regarded as a positively charged hole, and the electron in the conduction band gives a hydrogen - like spectrum with an infinitive number of bound state and ionization continuum (see Figure 2 in ref. [34]). Below we will briefly describe the results of the optical spectroscopy of isotope - mixed solids. In our experiments we have investigated the low - temperature luminescence spectra of LiH_xD_{1-x} crystals ($0 \leq x \leq 1$) which are differ by term of one neutron from each other as well as an allotrope of diamond.

Photoluminescence is the optical radiation emitted by a physical system (in excess of the thermal equilibrium blackbody radiation) resulting from excitation to a nonequilibrium state by irradiation with light. Photoluminescence is also rapidly evolving into major basic research tool comparable to absorption (reflection) measurements in importance. Two reasons for this stand out as significant. First is the sensitivity of the luminescence technique. It often happens that features which are just discernible in absorption will completely dominate the luminescence spectra. The converse is also sometimes true, making luminescence and absorption (reflection) complementary techniques. Second is the simplicity of data collection. In last half- century the luminescence method has become one of the most common techniques for studying excitons in dielectrics and semiconductors. While the structure

of spectra of fundamental reflection (absorption) depends on the internal degrees of freedom of Wannier-Mott exciton, the structure and shape of the luminescence spectrum are determined primarily by its external degrees of freedom. The latter are associated with the translation motion of large – radius exciton as a whole, with the translation mass $M = m_e + m_h$, where m_e and m_h – effective masses of electron and hole, respectively.

A) LiH

As demonstrated earlier [27], most low - energy electron excitation in LiH (LiD) crystals are large - radius excitons (see also [33]). Exciton luminescence is observed when LiH crystals are excited in the midst of fundamental absorption. The spectrum of free excitons of LiH crystals cleaved in superfluid helium consists of narrow (in the best crystals, its half - width is $\Delta E \leq 10$ meV) phononless emission line and its broader longitudinal optical (LO) phonon repetition, which arise due to radiated annihilation of free excitons with production of one to five LO phonons (see Figure 1 in Ref. [30]).

The isotopic shift of the zero - phonon emission line of LiD crystals equals 103 meV. As we can see from Figure 1 (Reference [30]) the photoluminescence spectrum of LiD crystals is largely similar to the spectrum of intrinsic luminescence of LiH crystals. There are, however, some distinctions one is related. Firstly, the zero - phonon emission line of free excitons in LiD crystals shifts to the short - wavelength side on 103 meV. These results directly show the violation of the strong conclusion that the strong force does not act on leptons. The second difference concludes in less value of the LO phonon energy, which is equal to 104 meV.

When light is excited by photons in a region of fundamental absorption in mixed LiH_xD_{1-x} crystals at 2 K, line luminescence is observed (Figure 2), like in the pure LiH and LiD crystals. As before [27 - 29], the luminescence spectrum of crystals cleaved in superfluid liquid helium consists of the relatively zero - phonon emission line and its wide LO replicas. For the sake of convenience, and without scarfing generality, Figure 2 shows the lines of two replicas. Usually up to five LO (sometimes 6) repetitions are observed in the luminescence spectrum of the free excitons as described in detail in [35]. In Figure 2 we see immediately that the structure of all three spectra is the same. The difference is in the distance between the observed lines, as well as in the energy at which the luminescence spectrum begins, and in the half - width of the lines.

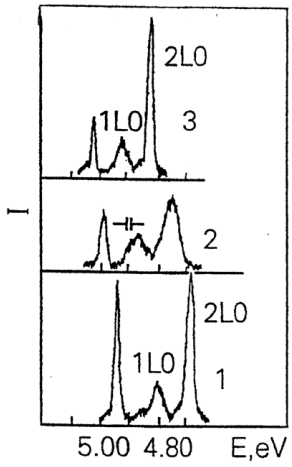

Figure 2: Photoluminescence spectra of free excitons in LiH (1), LiH_xD_{1-x} (2) and LiD (3) crystals cleaved in superfluid helium at 2 K. Spectrometer resolution is shown

The X - ray diffraction investigations show that the LiH_xD_{1-x} mixed crystals [36] form a continuous row of the solid solution and testify themselves like a virtual crystal with a variable lattice constant (and exciton radius, respectively) that obeys Vegard's law (see Figure 3).

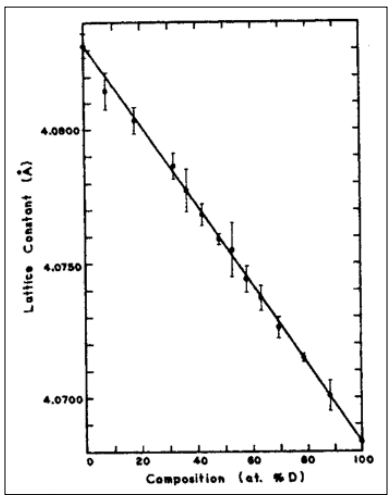

Figure 3: Lattice constant in the $^7Li(H,D)$ crystals plotted against the isotopic composition [36]

The measurements of the low temperature of reflection [27,9] and luminescence spectra of the whole series of mixed crystals is permitted to obtain the dependence of the interband transition (the long - range force dependence of strong nuclear interaction on the distance between nucleons in deuterium nucleus) energy on the deuterium concentration (see above Figure 4). Taking into account that the concentration of the isotopes is vary directly the lattice constant (see Figure 3) we are plotting the dependence of the power of the force strong interaction on the distance between nucleons depicted on Figure 4 This dependence has a nonlinear character. As can be seen from Figure 4, VCA method (the straight dashed line) cannot describe observed experimental results.

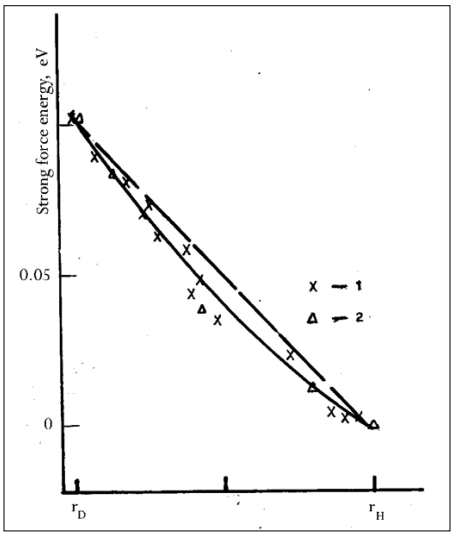

Figure 4: The long-range part of the force of strong nuclear interaction dependence on the distance between nucleons in deuterium nucleus. The straight dashed line is the linear dependence of the force dependence F_s in the virtual model. The solid line corresponds to calculation using the polynom of second-degree $F_s = f(r_d)$. Points derived from the reflection spectra indicated by crosses, and those from luminescence spectra by triangles

Comparison the experimental results on the luminescence (reflection) and light scattering [27,9] in the crystals which differ by a term of one neutron only is allowed to the next conclusions;

1. At the adding one neutron (using LiD crystals instead LiH ones) is involved the increase the valence band - to conduction band transition energy on 103 meV (see, also [37]).
2. At the addition one neutron the energy of LO phonons is decreased on the 36 meV that is direct seen from luminescence spectra [27].
3. In the isotope effect, the energy of acoustic phonons does not depend on the replacement of H by D [27], which is proved by the identical structure of the light scattering spectra. Along with this, a small change in the energy of optical (LO) phonons (36 meV) observed in the luminescence and light scattering spectra indicates a non - electron - phonon renormalization mechanism of the energy of zero - phonon emission line of free excitons in LiD crystals. These results are forcing us to search for new models and mechanisms of nuclear - electron interaction including results of subatomic physics, e.g. hadron - lepton interaction.

Traditionally nuclear - electron interaction (in our case neutron - electron interaction) taking into account the solving of Schrodinger equation using a model of Born - Oppenheimer (adiabatic) approximation [38]. Since electrons are much faster and lighter than the nuclei by a factor nearly 2000 the electron charge can quickly rearrange itself in response to the slower motion of the nuclei, and this is the essence of the Born - Oppenheimer approximation. This approximation results the omission of certain small terms which result from the transformation. As was shown in [39] the eigenvalue (energy) of the electronic Schrödinger equation depends on the nuclear charges through the Coulomb potential, but it doesn't include any references to nuclear mass and it is the same for the different isotopes. The independent of the potential energy (the eigenvalue of the Schr õdinger equation) is the essence adiabatic approximation. However, we must repeat, that the Born - Oppenheimer approximation is the standard anzatz to the description of the interaction between electrons and nuclei in solids [32]. Now we should take into account a small contribution to isotopic shift through reduced electron mass $\mu = [(m_e M_{Nucl}) / (m_e + M_{Nucl})]$ so far as M_{Nucl} is different for the hydrogen and deuterium nucleus. In this case the contribution equals $\Delta E = 6$ meV. Contribution to isotope shift of the zero - phonon line in luminescence spectra of LiD crystals as well as Lamb shift and specific Coulomb potential approximately equal 1, and 1 meV, respectively. This value is less then isotope shift in our experiments on the two order and more. We should repeat that all these results are forcing us to search for new models and mechanisms of nuclear - electron (in our case neutron - electron) interaction including results of subatomic physics, e.g. hadron - lepton interaction [8] Following to the results [40] we assume that in our tentative interpretation of our experimental results the electromagnetic origin (magnetic - like long - range interaction between neutron quarks and leptons (electrons)). We should add, that this phenomenon of quark confinement is, even today not properly understood [8]. Our estimation for the Yukawa radius equal to $a_0 = 0.53 \quad 10^{-10}$ m the related mass of the intermediate new kind particle (boson) is 3.5 keV which interact with hadron (neutron in deuterium nucleus) and lepton (electron). In electrostatic model it was shown [41] that the interaction of a neutron with an electron is less than an analogous proton with an electron by approximately 128 times. Hence it follows that the theoretical value of the binding energy of a neutron with an electron is 106.7 meV. the value of the neutron - electron binding energy found by us in the experiment, equal to 105 meV, is in excellent agreement with theoretical value.

B) Diamond

Carbon, one of the most elements in Nature still gives a lot of surprises. It is well known that isolated carbon atoms have the electronic configuration $1s^2$, $2s^2 2p^3$ (see, e.g. [42]). However, in the diamond crystal as a result of the formation of the sp^3 hybrid (a mixture of 2s and 2p wavefunction with tetrahedral bonding) there is a modification of the s - and p - levels which manifests itself in a further splitting of the sp^3 hybrid band into two bands, each of which (including spin) can accommodate four electrons. The four electrons of the atomic 2s - and 2p - states thus fill the lower part of the sp^3 band leaving the upper part unoccupied. Between the two sp^3 subbands there is a forbidden energy gap of width E_g. This is the origin of the insulating property of diamond.

Carbon atom is built from 6 protons, A neutrons and 6 electrons, where A = 6 or 7, yield the stable isotopes ^{12}C and ^{13}C, respectively, and A =8 characterizes the radioactive isotope ^{14}C. The isotope ^{12}C, with nuclear spin I = 0, is the most common one in nature with 99% of all carbon atoms, whereas only ~ 1% are ^{13}C with nuclear spin I = 1/2. There only traces of ^{14}C (10^{-12} of all carbon atoms) which β - decays into nitrogen ^{14}N. Although ^{14}C only occurs rarely, it is important isotope used for historical dating (see, e.g. [43]).

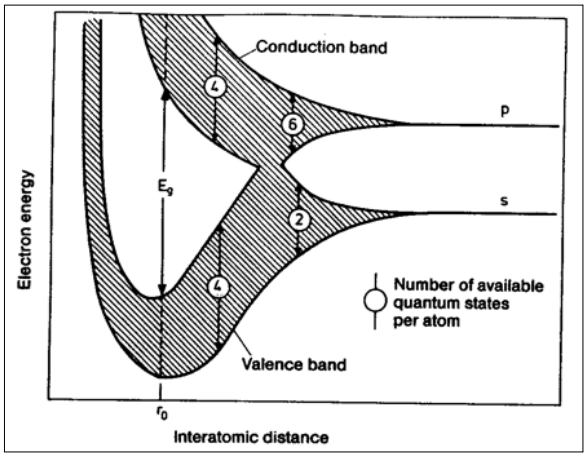

Figure 5: Schematic behavior of the energy bands as a function of atomic separation for the tetrahedrally bound semiconductor diamond (C). at the equilibration separation r_0 there is a forbidden energy gap E_g between the occupied and unoccupied bands that result from sp^3 hybrid orbitals. For diamond, sp^3 hybrid stems from the 2s and $2p^3$ atomic states. one sees from this figure that the existence of a forbidden energy region is not tied to the periodicity of the lattice.

Carbon, one of the most basic elements in nature, still gives a lot surprises. It is found in many different forms - allotropes - from zero-dimensional fullerene, one dimensional carbon nanotubes, two-dimensional graphene and graphite, to three-dimensional diamond (Figure 6) - and the properties of the various carbon allotropes can vary widely [44]. For instance, diamond is the hardest material, while graphite is one of the softest: diamond is transparent to the visible part of spectrum, while graphite is opaque; diamond is an electrical insulator, while graphite is a conductor. Very important is that all these different properties originate from the same carbon atoms, simply with different arrangements of the atomic structure.

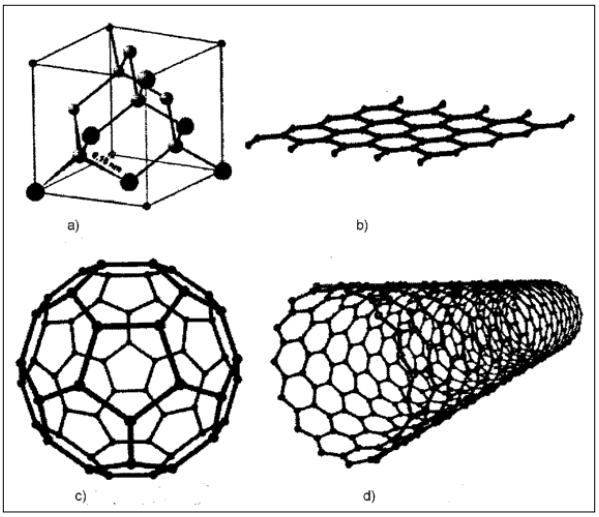

Figure 6: Structure of some Representative Carbon Allotropes

The Diamond is one of the simplest and most important systems, especially in isotope effect of condensed matter. It has considerable mechanical strength; also, it has high thermal conductivity and chemical stability even at several hundreds of degrees Celsius [45, 46]. Diamond has, perhaps, the simplest and most basic covalent band structure. Figure 7 shows the electronic energy - band along several lines of high symmetry from the center (Γ) to the boundary of the first BZ as calculated with modified LCAO method in paper [47].

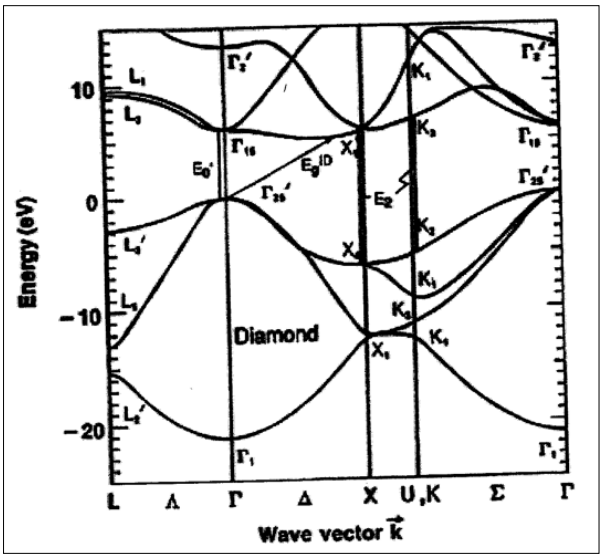

Figure 7: Electronic energy band structure of diamond along several lines of high symmetry from the center to the boundary of the first BZ as calculated with a modified LCAO method [47].

The electronic states are labeled using the notation for the single group of the diamond structure. The location of several interband transitions is included by the vertical arrows. The fundamental absorption edge of diamond corresponds to indirect transitions from highest valence band at the point to the lowest conduction band in the Δ direction (X point) (i.e., $\Gamma_{25} \rightarrow \Delta_1$ [X_1]). The

theoretical indirect gap energy E_g^{ID} lays between 5.05 and 5.6 eV

[48], that in reasonable agreement with the experimental data: E_g^{ID}= 5.470 ± 0.005 eV [45 46]. Like in Si, the lowest - lying conduction band at point of BZ in diamond, Γ_{15} is p - like, however, as we can see, in Ge the s - like Γ_2 band is the lowest conduction band. As mentioned in literature (see, e.g. [49] and references therein), one common characteristic of all published spectra in the UV region of diamond is the presence of two major peaks at ~ 7.02 - 7.4 eV and ~ 12.2 - 12.7 eV. The first peak may originate from transition (E_0') and the second one from $X_4 \rightarrow X_1$ and $\Sigma_2 \rightarrow \Sigma_3$ transitions (E_2) (the more detail see [45]).

Further we will briefly discuss dependence of the electronic gap (E_g) as well as phonon states of diamond with its isotopic composition. Figure 8 compares the edge luminescence for a natural diamond with that for a synthetic (^{13}C) diamond. The peaks labeled A, B and C due, respectively, to the recombination of a free exciton with emission of transverse - acoustic, transverse - optic and longitudinal - optic phonons having wave vector ± k_{min} [50, 51].

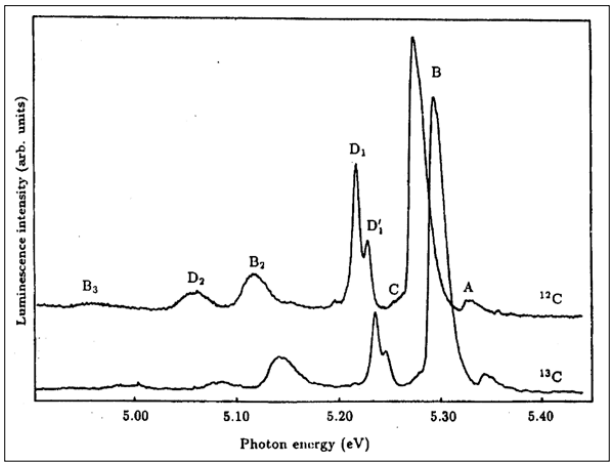

Figure 8: Cathodoluminescence spectra of ^{12}C and ^{13}C at 77 K [52].

As it can be seen from Figure 8 the band gap of ^{13}C has increased by 13.6 meV. Numerous examples of band gap increasment at hard isotope substitution were collected in the papers [50, 51]. More detail isotope renormalization of the band gap in diamond was investigated in the paper [53]. The results of these authors depicted on the Figure 9.

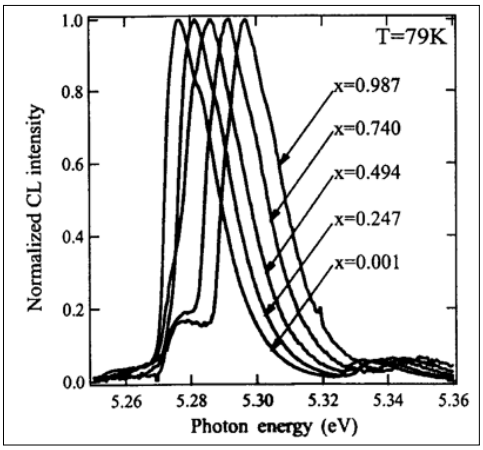

Figure 9: Luminescence spectra of free excitons in homoepitaxial diamond films grown from mixture of methane in hydrogen by means of a microwave plasma - assisted CVD. The spectra illustrate the effects of isotope composition (x = 0.001; 0.247; 0.494; 0.740; and 0.987) mixed in the CVD gas phase. All spectra

are normalized to the same height (after [53]).

Watanabe et al. have concluded that the maximum change of the band gap due to substitution of ^{12}C by ^{13}C is $\Delta E_g = 15.4$ meV. This value per one neutron and on seven neutrons we get 15.4 x 7 ≃ 108 meV. This value is very close to the observed of neutron - electron binding energy in LiD crystals.

The effect of the isotopic ^{12}C to ^{13}C ratio on the first and second - order Raman scattering of light in the diamond has been investigated in [54]. As the ^{13}C content is increased from the natural ratio (^{12}C to $^{13}C = (1 - x) / x$, where $x = 0.011$), to the almost pure ^{13}C ($x = 0.987$), the whole spectrum has shifted towards longer wavelengths (see Figure 10) in good agreement with the expected M-0.5 frequency dependence on the reduced mass M. For an approximately equal mix of the two isotopes, the authors reported that the features seen in the above two - phonon spectra were either broadened or unresolvable. We should stress that the main line in the first - order Raman scattering spectrum of light at $\omega = 1332$ cm^{-1} also shifts to the short-wavelength side on the 52.3cm^{-1} [54].

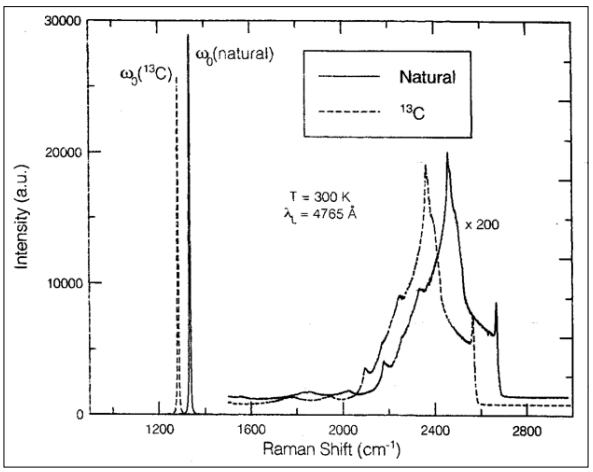

Figure 10: The Raman spectrum of a natural and a ^{13}C diamond. The spectra show the dominant first - order, Raman - active F_{2g} line and the significantly weaker, quasi - continuous multi - phonon features [54].

The above experimental results on the basis of different substances and with different structures simple prove the renormalization of the energy of elementary exctiations (electrons and phonons by strong nuclear interactions. The heuristics of mechanism of the strong nuclear interaction in the model of hadron mechanics [9^b] undoubtedly deserves deep study and continuation of this direction. It should be added in this regard that more than a century ago [89] the insufficiency of the point model of elementary particle has been emphasized (see also [90, 29]).

C) Graphene

In two-dimensional graphene, carbon atoms are periodically arranged in an infinite honeycomb lattice (Figure18 in [55]). Such an atomic structure is defined by two types of bonds within the sp2 hybridization. From the four valence orbitals of the carbon atom (the 2s, 2px, 2py, and 2pz orbitals, where z is the direction perpendicular to the sheet), the (s, px, py) orbitals combine to form the in-plane σ (bonding or occupied) and σ* (antibonding or unoccupied) orbitals. Three σ-bonds join a C atom to its three neighbors. They are quite strong, leading to optical - phonon frequencies much higher than observed in diamond (see below). Such orbitals are even with respect to the planar symmetry. The σ bonds are strongly covalent bonds determining the energetic stability and the elastic properties of graphene. The remaining pz orbital, pointing out of the graphene sheet is odd with respect to the planar symmetry and decoupled from the σ states. From the lateral interaction with neighboring pz orbitals (called the ppπ interaction), localized π (bonding) and π* (antibonding) orbitals are formed [56]. Graphite consists of a stack of many graphene layers. The unit cell in graphite can be primarily defined using two graphene layers translated from each other by a C - C distance ($a_{C\text{-}C}$ =1.42 Å). The three-dimensional structure of graphite is maintained by the weak interlayer van der Waals interaction between π bonds of adjacent layers, which generate a weak but finite out-of-plane delocalization [55]. The bonding and antibonding σ bands are actually strongly separated in energy 12 eV at, and therefore their contribution to electronic properties is commonly disregarded, while the bonding and antibonding π states lie in the vicinity of the Fermi level (Figure 11). The two remaining π bands completely describe the low energy electronic excitations in both graphene and graphite (see [4] and references therein). The bonding π and antibonding π* orbitals produce valence and conduction bands (Figure 11) which cross at the charge neutrality point (Fermi level of undoped graphene) at vertices of the hexagonal Brillouin zone. Carbon atoms in a graphene plane are located at the vertices of a hexagonal lattice.

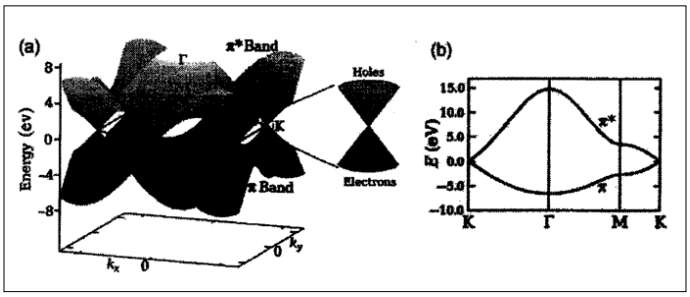

Figure 11: Energy dispersion of graphene obtained within the tight - binding approximation. a) Energy dispersion relation for graphene, drawn in the entire region of the Brillouin zone. Since in this approximation to ignore the coupling between the graphene sheets, the bands depend only on kx and ky. The π band is completely filled and meets the totally empty π^* band at the K points. Near these points both bands linear dispersion as described in the literature. b) The dispersion along the high symmetry points ΓMK.

This graphene network can be regarded as a triangular Braves lattice with two atoms per unit cell (A and B). Each A - or B - type atom is surrounded by three atoms of the opposite type. In a simple neighbor model graphene is a semimetal with zero - overlap between valence and conduction bands. The energy dispersion of π electrons in graphene was first derived in 1947 by Wallace [56] within the tight - binding approximation. In this case, the wave function of graphene is a linear combination of Bloch function for sublattice A

$$\Phi_A = \frac{1}{\sqrt{N}} \sum_{\vec{R}_A} e^{i\vec{k}\vec{R}_A} \varphi(\vec{r} - \vec{R}_A), \quad (2)$$

and equilibrium function Φ_B for the B sublatice. Here N is the number of unit cells, $\vec{R}_A$ are the position of the atom A and $\varphi(\vec{r} - \vec{R}_A)$ is the 2pz orbital of the atom at $\vec{R}_A$. The sum runs over all unit cells, i.e. all possible lattice vectors. In the nearest neighbor approximation

(every A site has three nearest B sites, and vice versa), the energy eigenvalues can be obtained in a closed form [56, 55].

$$\varepsilon(k_x, k_y) = \pm \gamma_0 \left[1 + 4\cos\frac{\sqrt{3}k_x a}{2}\cos\frac{k_y a}{2} + 4\cos^2\frac{k_y a}{2}\right]^{1/2}, \quad (3)$$

where γ_0 is the transfer integral between the nearest neighbors. The energy dispersion of two - dimensional graphene according to this formula is plotted in Figure 11(a) as a function of the wave vector $\vec{k}$. The upper half of the curves is called the π* or the antibonding band while the lower one is π or the bonding band. The two bands degenerate at the two K points given by the reciprocal space vectors $\vec{K} = (2/a)(1/3, 1/\sqrt{3})$ and $\vec{K}' = (2/a)(-1/3, 1/\sqrt{3})$ points where the dispersion vanishes (see above).

Basically, graphene has redefined the limits of what a material can do: it boasts record thermal conductivity and the highest current density at room temperature ever measured (a million times that of copper!); it is the strongest material known (a hundred times stronger than steel!) yet is highly mechanically flexible; it is the least permeable material known (not even helium atoms can pass through it!); the best transparent conductive film; the thinnest material known; and the list goes on ...[55]. In the vicinity of K - points (as it can be seen from Figure 11), the low - energy electron/hole dispersion relation is proportional to momentum, rather than its square. This is analogous to the energy dispersion relation of massless relativistic electrons, so the electrons/holes of graphene are described as Dirac fermions having no mass. In a simple neighbor model graphene is a semimetal with zero - overlap between valence and conduction bands. In order to make graphene a real technology, a special issue must be solved: creating an energy gap at K - points in the Brillouin zone. Different attempts have been made by researches, such as patterning graphene into nanoribbon [57], forming graphene quantum dots [58-60], making use of multilayer graphene sheets [61, 62] and applying an external electric field [63]. It was shown that the uniaxial strain can open a band - gap in a metallic carbon nanotube as well as carbon nanoribbon [64].

Elastic and inelastic light scattering are powerful tools for investigating graphene [65 - 70]. Raman spectroscopy allows monitoring of doping, defects, disorder, chemical and isotope [50, 51] modifications, as well as edges and uniaxial strain. All sp^2 - bonded carbons show common features in their Raman spectra, the so - called G and D peaks (see, e.g. Figs. 16 18 in [55]), around 1580 and 1360 cm^{-1} (see, e.g. [66, 67]). The G peak (see, also below Figure13) corresponds to the E_{2g} phonon at the Brillouin zone center (Γ- point). The D peak is due to the breathing modes of six - atom rings and requires a defect for its activation. It comes from TO phonons around the Brillouin zone K point and it is activated by an intravalley scattering process [66]. The 2D peak is the second order of the D peak. This is a single peak in monolayer graphene, whereas it splits into four bands in bilayer graphene, reflecting the evolution of the band structure [67]. The Raman spectrum of graphene also shows significantly less intensive defect - activated peaks such as the D' peak, which lies at ~1620 cm^{-1}. This is activated by an intravalley process i.e. connecting two points belonging to the same cone around K (see, Figure 11) [67]. The second order of the D' peak is called 2D' peak. Since 2D and 2D' peaks originate from a Raman scattering process where momentum conservation is obtained by the participation of two phonons with opposite wave vector ($\vec{q}$ and - $\vec{q}$), they do not require the presence of defects. Thus, they are always visible in the Raman spectrum (see cited papers [65-70] and references therein).

Graphene is one unique material which shows properties not fond in other materials. One of these unique features of graphene is the influence of long-range strains on the electronic properties. The possibility of tuning the dynamics of carriers as well as phonons by appropriately designed strain patterns opens the way for novel applications of graphene, not possible with any other materials (see, e.g. [71] and references therein). At present time we have several reports, which have examined graphene properties under uniaxial deformation [64, 70-72].

Strain can be very efficiently studied by Raman spectroscopy since this modifies the crystal phonon frequency, depending on the anharmonicity of the interatomic potentials of the atoms. Raman spectra of strained graphene show significant redshifts of 2D and G band (see Table 1) because of the elongated of the carbon - carbon bonds.

Table 1: Red Shift of the G and 2D bands in the Raman Spectra in Graphene Monolayers Under Uniaxial Tensile Stress

Ref.	Shift of G (G^+ and G^-) band cm^{-1}/%	Shift of 2D band cm^{-1}/%	E_g, meV
16	14.2	27.8	300
70	5.6; 12.5	21	
72	10.8; 31.7	64	
71			
theory			≃ 500

The authors of the paper [64] have proposed that by applying uniaxial strain on graphene, tunable band - gap at K - point can be realized. First principal calculations predicted a band - gap opening of 300 meV for graphene under 1% uniaxial tensile strain (Figure 12). Thus, the strained graphene provides an alternative way to experimentally tune the band - gap of graphene, which would be more efficient and more contollable than other methods (see, above) that are used to open band - gap in graphene.

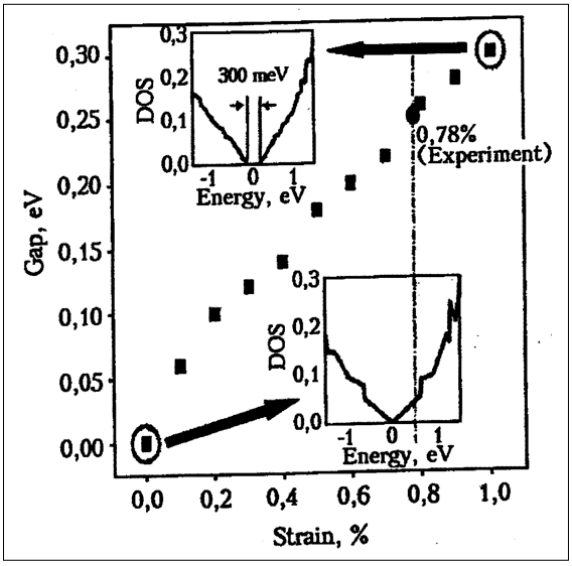

Figure 12: The band - gap of strained graphene with the increase of uniaxial tensile strain on graphene. The magnitude of gap is determined by the gap opening of density of states. The inserts show the calculated density of states of unstrained and 1% tensile strained graphene. The dash line and solid dot indicate the calculated bandgap of graphene under the highest strain (0.78 %) [64].

The method of the isotope renormalization of the energy of elementary excitations in solid very often used in last five decades and well described in the scientific literature (see, for example reviews [50, 51, 55]). At now there is a large list of the paper devoted to investigation of the isotope - mixed graphene [60, 65, 73 - 77]. Chen at al. [68] have reported the first experimental study of the isotope effect on the thermal properties of graphene. The thermal conductivity K, of isotopically pure ^{12}C (0.01 of ^{13}C) graphene determined was higher than 4000 W/mK (approximately two times more than it in diamond [63]) at the measured temperature T_m~ 320K, and more than a factor of two higher than the value of K in a graphene sheets composed of a 50% - 50% mixture of ^{12}C and ^{13}C. Raman spectroscopy transferred to the 285 nm SiO_2/Si wafer was performed under 532 nm laser excitation [68]. The G peak and 2D band positions in Raman spectra of graphene with 0.01%, 1.1%, 50% and 99.2% ^{13}C - isotope are presented in Figure 13.

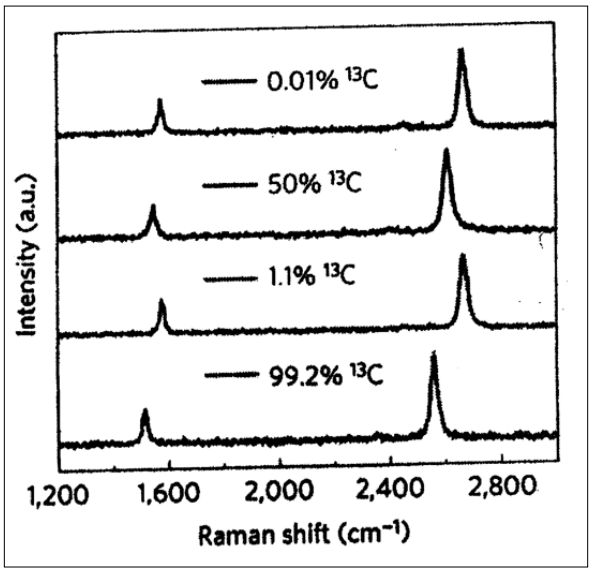

Figure 13: Raman Spectra of Graphene with different Isotope Concentration at room Temperature [78].

Isotope shift of the G and 2D bands in the Raman spectra depicted on the Figure14 [78].

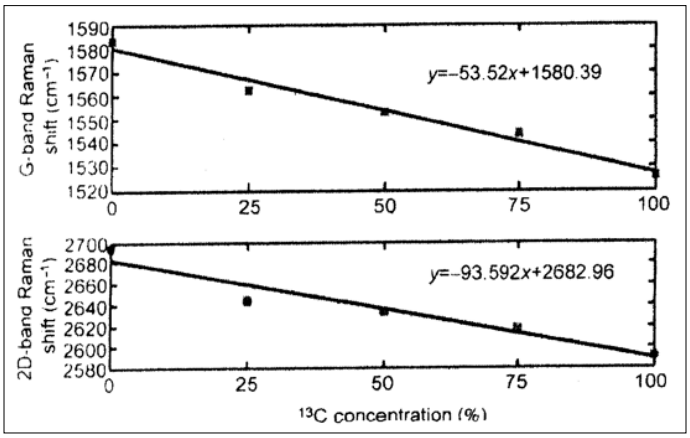

Figure 14: Peak position of G and 2D bands in Raman spectra as a function of the concentration of ^{13}C [78].

As in the case of isotope - mixed diamond [50, 51] the Brillouin - zone - center optical - phonon frequency ω varies with the atomic mass M as $\omega \sim M^{-1/2}$ making the Raman shift for ^{13}C approximately $(12/13)^{-1/2}$ times smaller than that for ^{12}C. The experimental difference between the lowest 99.2% ^{13}C and the highest 0.01% ^{13}C peak is ~ 64 cm^{-1} which is according [67, 68] in agreement with the theory, and attests for the high quality of isotopically modified graphene. By the way we should indicate that in the Raman spectra in diamond (with sp^3- bond) analogous shift of first - order line in Raman spectrum is equal 52.3 cm^{-1} [79], which is consistent with the isotope mass ratio. Substituting a light isotope (^{12}C, H) with a heavy one increases the interband transition energy in the case $^{12}C_x\,^{13}C_{1-x}$ on 14.7 meV and LiH_xD_{1-x} on 103 meV [50]. Taking into account a softer bond (sp^2 - bond instead sp^3 - bond in diamond) isotope - induced band - gap opening in graphene of some hundreds meV (up to E_g of Si) was predicted in paper [60]. Such estimation of the value of isotopical band - gap opening in graphene agrees with not only the results of paper [79] but with very small value $C_{44} = 0.5 \cdot 10^{10}$ dyn/cm^2. Such small value indicates on the strong electron - photon interaction - main reason renormalization of electron excitation energy (for the details, see, e.g. [39]). Very close to isotopically renormalization of electronic excitation energy is the hydrogenation of graphene [60]. In last mechanism there is observable band - gap opening in graphene. We should add that use deuterium instead of hydrogen we may increase the value of E_g [50]. Thus, isotope substitution will be very useful method for renormalization of the band - gap in graphene - future semiconducting material. Moreover, this method allows to control not only of the strong nuclear interaction (quantum chromodynamics) but taking it into account at the renormalization of the electromagnetic interaction (quantum electrodynamics) [50, 51]. Adding ^{13}C makes magnetic materials isotope out of graphene.

In conclusion let's discuss neutron - electron interaction [19]. There is a common place in Standard Model of modern physics that the strong nuclear force does not act on leptons [7]. Numerous experimental results of the isotope effect study in solids [50, 51, 55] show the violation of this strong conclusion. Really, traditionally nuclear - electron (in our case neutron - electron) interaction taking into account the solving of Schrödinger equation (see, e.g. [39]) using Born - Oppenheimer (adiabatic) approximation [38]. This approximation results the omission of certain small terms which result from the transformation. As was shown in [39] the eigenvalue (energy of the electronic Schrödinger equation (equation 6 in [39])) depends on the nuclear charges through the Coulomb potential, but it does not include any references to nuclear mass and it is the same for the different isotopes. This result is forcing us to search for new models and mechanisms of nuclear - electron interaction including the results of subatomic physics [6], e.g. hadron - lepton interaction (see also [80]). We should remind that the Standard Model of particle physics (theory of strong interaction) assumes the conservation of lepton and baryon numbers separately, and there no processes that convert quarks to leptons. This means that the Standard Model itself does not prohibit the possibility that the charge of the electron and the proton are slightly different [6]. On the other hand, the neutron comprising quarks can decay into a proton, an electron, and a neutrino. Therefore, a charge asymmetry between the proton and electron would be linked to the charge of the neutron. (see, also [81]). The experimental results of isotope effect evidence the long - range strong interaction [28]. Thus, the use of the method of isotope effect in graphene may throw light on the renormalization of the mass of massless fermion in graphene as well as unification of forces (see, e.g. [40, 82]).

The remarkable properties of the graphene promise unheard of applications, especially in the semiconductor state. Especially graphene nanostructures are promising candidates for future nanoelectronics and solid - state quantum information technology. As was shown numerously, in the vicinity of K - points (Figure 11), the low - energy electron/hole dispersion relation is proportional to momentum, rather than its square (see, e.g. [55]). This is analogous to the energy dispersion relation of massless relativistic electrons, so the electrons/holes of graphene are described as Dirac fermions having no mass. In a simple neighbor model graphene is a semimetal with zero - overlap between valence and conduction bands. In order to make graphene a real technology, a special issue must be solved: creating an energy gap at K - points in the Brillouin zone (see, Figure 15).

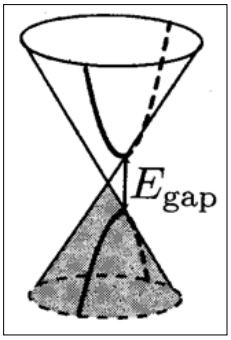

Figure 15: The Energy Dispersion of Semimetal (Solid Line) and Semiconductor (Dashed Line)

Different attempts have been made by researches, such as patterning graphene into nanoribbon, forming graphene quantum dots, making use of multilayer graphene sheet and applying an external electric field [62]. It was shown that the uniaxial strain can open a band - gap in a metallic carbon nanotube as well as carbon nanoribbon. As an example, Figure 16 shows the dependence of the energy of interband transition on the width of the graphene nanoribbons. The observed dependence is well described by the following expression $E_g = \alpha^* / (W - W^*)$, where $\alpha^* = 0.38$ eV/nm, and $W^* = 16$ nm accounts for inactive edges [83]. This formula gives value of E_g equal to several eV, if W is reduced to a size, for example, ^{13}C, but it is impossible. The isotopic transformation of graphene, a semimetal into semiconductor deserves special attention [84]. This means of the cone's dispersion pattern E ($\vec{k}$) at the K point of the Brillouin zone of graphene reformes into the usual parabolic dispersion of band structure pattern (see Figure 16).

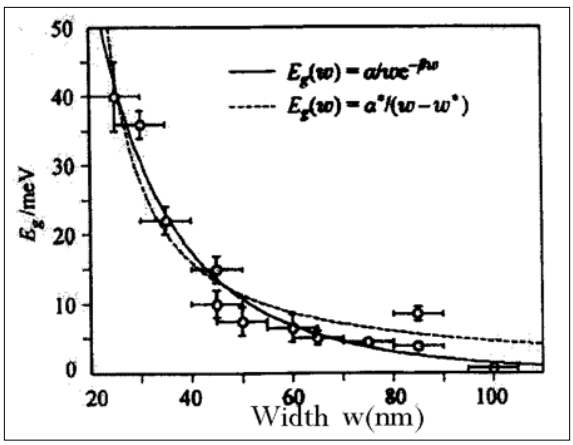

Figure 16: The Dependence of Eg as a function of width of the Graphene Nanoribbons (after [83])

According to the results of Ref. 85 this method can be used to obtain Eg of several hundred meV. since value of Eg depends on the concentration of ^{13}C in graphene, this mechanism is easily realized either chemically or technologically. With the opening Eg of massless fermions (leptons = electrons) acquire mass. Estimates of different ways of opening Eg in graphene give the following equality: Eg = 2m [84]. When Eg = 1 eV leptons acquire a mass equal 0.5 eV - the value is not large, but finite [85]. One of the mechanisms of acquire mass in elementary particle physics is considered in the paper [86]. This paper predicts that both quarks and gluons acquire running mass distribution in QCD, which are large at infrared momenta. The current quark of perturbative QCD evolves into a constituent quark as its momentum becomes smaller. The constituent quark mass arises from a cloud of low - momentum gluons attaching themselves to the current quark. This is DCSB (dynamical chiral symmetry breaking): an essentially nonperturbative effect that generates a quark mass from nothing; namely it occurs even in the chiral limit. DCSB namely the generation of mass from nothing is a theoretically established nonperturbative feature of QCD. The solution of a gap equation shows that gluons are cannibals: they are particle species whose members become massive by eating each other (the details see [86 - 90]).

Conclusion

The isotope effect is a macroscopic manifestation of a strong nuclear force. The successful use of low - temperature atomic spectroscopy of a solid manifested new properties of nuclear strong interaction. The latter allows us to talk about the solid manifestation of quantum chromodynamics.

Acknowledgements

Many thanks G.A. Plehhanov for improving my English.

References

1. Mochalov VV (2023) Investigation of spin effects on nuclear targets at the U - 70 accelerator complex. Book of Abstracs of 73 Int. Conf. NUCLEUS - 2023, Sarov, Russia: 15-16.
2. Jackson JD (1975) Classical Electrodynamics (J. Wiley and Sons, New-York, Chichester).
3. Chadwick J (1932) The existence of a neutron, Proc. Roy. Soc. (London) 136, 692-708.
4. Soddy F (1913) Nature 92 399, ibid, 92, 452.
5. A Garcia, Henley EM (2007) Subatomic Physics. World Scientific Publishing CO., Singapore. http://www.gammaexplorer.com/wp-content/uploads/2014/03/Subatomic-Physics.pdf.
6. Martin BR (2006) Nuclear and Particle Physics. Wiley and Sons Ltd.-VCH, Weinheim.
7. Cottingham WN, Greenwood DA (2007) Introduction to Standard Model of Particle Physics. Cambridge University Press, Cambridge. https://www.cambridge.org/core/books/an-introduction-to-the-standard-model-of-particle-physics/82428B02F3EE6E45113421D2386B29A1
8. Perkins DH (2000) Introduction to High Energy Physics. Cambridge University Press, Cambridge. https://www.cambridge.org/core/books/introduction-to-high-energy-physics/2164D77FA13CC52D8B32130CF897E764
9. Plekhanov VG (2023) Dependence of the Yukawa potential on the distance between nucleons. Prog Chem Sci Research 7: 51-61.
10. Yukawa H (1935) On the interaction of elementary particles. Proc Phys Math Soc 17: 48-57.
11. Dee PI (1932) Attempts to detect the interaction of neutrons

with electrons. Proc Roy Soc A136: 727-736.
12. Condon EU (1936) Note on electron-neutron interaction. Phys Rev 49: 59-61.
13. Aronberg (1918) Astrophys. J 47: 96.
14. Striganov AP, Ju P Donzov (1955) Isotope effect in atomic spectra. Uspekhi Fiz. Nauk 55: 315-330.
15. King WH (1984) Isotope Shift in Atomic Spectra (Plenum Press, New York). https://link.springer.com/book/10.1007/978-1-4899-1786-7
16. Foldy LL (1952) The electromagnetic properties of Dirac particles. Phys Rev 87: 688-696.
17. Darwin CG (1928) The wave equation of electron. Proc Roy Soc A118: 654-680.
18. Yu A Alexandrov (1982) The Fundamental Properties of Neutron (Energoizdat, Moscow) (in Russian).
19. Foldy LL (1958) Neutron-electron interaction. Rev Mod Phys 30: 471-481.
20. Karshenboim SG (2010) Constraints on a long-range spin-independent interaction from precision atomic physics. Phys Rev D82: 073003-073006.
21. Delaunay C, Soreq Y (2016) Probing new physics with isotope shift spectroscopy 1-6.
22. Delaunay C, Ozeri R, Perez G (2017) Probinc atomic Higgs-like forces atthe precision frontier, Phys. Rev D 96: 093001-093007.
23. Berengut JC, Budker D, Delaunay C (2017) Probing new ligh force mediatore by isotope shift spectroscopy 1-13.
24. Frgiuele C, Fuchs E, Perez G (2017) Constraining new physics models withisotope shift spectroscopy, Phys. Rev D 96: 015011-11.
25. Berengut JC, Budker D, Delaunay C (2018) Probing new long - range interaction by isotope shift spectroscopy, Phys. Rev. Lett 120: 091801-091807.
26. EE Boos (2022) The SMEET formalism: the asis for finding deviations from the Standard Model, Phys.-Usp. Moscow 65: 653-676.
27. VG Plekhanov (2004) Giant Isotope Effect in Solids (Stefan University Press, LaJola, USA 1-61.
28. VG Plekhanov (2017) Isotope Effect-Macroscopic Manifestation of the Strong Interaction (LAMBERT, Academic Publishing, Saarbrucken, Germany in Russian 1-9.
29. VG Plekhanov (2022) Non - accelerator measurement of the long-range quark lepton interactions in solids. J Conden Matter Nucl Sci 36: 353-361.
30. VG Plekhanov (2019) Necessity addition, Phys.-Usp Moscow 61: 449-450.
31. D Pines (1963) Elementary Excitations in Solids (W.A. Benjamin Inc., New York 1-200.
32. RM Martin (2004) Electronic Structure - Basic Theory and Practical Methods (Springer, Heidelberg 1-624.
33. R.S. Knox (1963) Theory of Excitons (Academic Press, New York-London https://onlinebooks.library.upenn.edu/webbin/book/lookupid?key=olbp92940
34. VG Plekhanov (2023) Non - accelerator study of the strong interaction dependence on the distance between nucleons, Hadronic Journal 46: 143-156.
35. VG Plekhanov (2001) Comparative study of isotope and chemical effects on theexciton states in LiH crystals, Prog. Sol. State Chem 29: 71-177.
36. WB Zimmerman (1972) Lattice constant dependence on isotopic composition inthe ^{7}Li (H, D) system, Phys. Rev B5: 4704-4707.
37. VG Plekhanov (2021) Experimental study of the long - range nuclear interaction insolids, Chapter 1 in, Understanding Quarks Nova Science Publishers Inc., New York 1-156.
38. M Born, H Kun (1954) Dynamical Theory of Crystal Lattices (Clarendon Press, Oxford https://en.wikipedia.org/wiki/Dynamical_Theory_of_Crystal_Lattices
39. VG Plekhanov (2019) Measurements of the wide value range of strong interaction coupling constant, SSRG-IJAP 6: 32-37.
40. FO Barut (1986) Unification based on electromagnetism, Annalen Phys. (Leipzig) 98: 83-92.
41. Breit G (1951) Electron-neutron interaction, Proceed. NAS 37: 837- 846.
42. Harrison WA (1980) Electronic Structure and Propertis of Solids (W.F. Freemanand Co., San Francisco).
43. Plekhanov VG (2012) Isotopes in Condensed Matter https://link.springer.com/book/10.1007/978-3-642-28723-7.
44. Dresselhaus MS, Eklund PC (2000) Phonons in carbon nanotubes. Advances in Physics 49: 705-814.
45. Vavilov VC, Gippius AA, Konorova EA (1985) Electron and optical processes in diamond. https://ui.adsabs.harvard.edu/abs/1985MoIzN..R....V/abstract
46. Mildren RP, Ratenau JR (2013) Intrinsic optical properties of diamond. Optical Engineering of Diamond: 1–34. https://onlinelibrary.wiley.com/doi/10.1002/9783527648603.ch1
47. Chelikowsky JR, Louie SG (2013) First - principles linear combination of atomic orbitals method for the cohesive and structural properties of solids: Application to diamond 29: 3470-3482.
48. Hybertsen MS, Louie SG (1986) Electron correlation in semiconductors and insulators: Band gaps and quasiparticle energies. Phys Rev B 34: 5390-5413.
49. Yu PY, Cardona M (1996) Fundamentals of Semiconductors. Physics and Materials Properties https://link.springer.com/book/10.1007/978-3-642-00710-1
50. Plekhanov VG (2005) Elementary excitations in isotope - mixed crystals. Physics Reports 410: 1-235.
51. Cardona M, Thewalt MLW (2005) Isotope effect on optical spectra of semiconductor 77: 1173-1224.
52. Collins AT, Lawson SC, Davies G, Kanda H (1990) Cathodoluminescence investigation of isotope effect in diamond. Phys. Rev. Lett 65: 891-893.
53. Watanabe H, Koretsune T, Nakashina S, Shikata S, Saito S (2013) Isotope composition dependence of the band - gap in diamond. Phys Rev B 88: 205420-205425.
54. Ramdas AK, Rodriguez S (1990) lattice vibrations and electronic excitation in isotopically controlled diamonds. Phys Stat Sol (b) 215: 71-80.
55. Ferrari AC, Bjnaccorso F, Fal'ko, Jari Kinaret, Tomas Löfwander, et al. (2015) Science and technology roadmapfor graphene, related two - dimensional crystals, and hybrid systems. Nanoscale 7: 4598-4810.
56. Wallace PR (1947) The band theory of graphite. Phys Rev 71: 622-629.
57. Han MY, Ozyilmaz B, Zhang Y, Philip Kim (2007) Energy band-gap engineering of graphene nanoribbons. Phys Rev Lett 98: 206805.
58. Ponomarenko LA, Schedin F, Katsnelson M, Yang R, Hill EW, et al. (2008) Chaotic Dirac billiard in graphene quantum dots. Science 320: 356-358.
59. Savchenko A (2009) Transforming graphene. Science 323: 589-590. Elias DC, Nair RR, Mohiuddin TMG, Novoselov KS, A K Geim, et al. (2009) Control of graphene properties by reversible hydrohenation: Evidence for graphane, ibid 323: 610-613.
60. Plekhanov VG (2011) Nuclear technology creation the quantum dots in graphene, Transactions Humanitar Institute, Tallinn 66-70.
61. See special issue Nature, June 11 (2009). https://www.nature.

com/nature/volumes/459/issues/7248
62. Mak KF, Lui CH, Heinz T F (2009) Observation of an electric - field - inducedband gap in bilayer graphene by infrared spectroscopy. Phys Rev Lett 102: 256405-256409.
63. Castro EV, Novoselov KS, Morozov SV, Peres NMR, Lopes dos Santos JMB, et al. (2007) Biased bilayer graphene: semiconductor with a gap tunable by the electric field effect. Phys Rev 99: 216802-216804.
64. H Ni Zh, Yu T, Lu YH, Wang YY, Feng YP et al. (2008) Uniaxial strain on graphene: Ramanspectroscopy study and band - gap opening. ACS Nano 3: 483-492.
65. Prawer S, Nemanich RJ (2004) Raman spectroscopy of diamond and doped diamond, Phil Transac R Soc (London) 362: 2537-2565.
66. Dresselhaus MS, Dresselhaus G, Hofman M (2008) Raman spectroscopy as a probe of graphene and carbon nanotubes. ibid, 366: 231-236.
67. Casiraghi C, Hartschuh A, Qian H, Georgi C, Fasoli A, et al. (2009) Raman spectroscopy of graphene edges. Nano Lett 9: 1433-1441.
68. Chen S, Wu Q, Mishra C, Kang J, Zhang H, et al. (2011) Thermal properties of isotopically engineered graphene. Nature Mater 11: 203-207.
69. Ferrari A (2007) Raman spectroscopy of graphene and graphite: Disorder, electron- phonon coupling, doping and nonadiabatic effects. Solid State Commun 143: 47-57.
70. Huang M, Yan H, Chen C, Heinz TF, Hone J, et al. (2008) Raman spectroscopy of graphene under uniaxial stress: phonon softening and determination of crystallographic orientation. Proc Natl Acad Sci USA 106: 7304-7315.
71. Farjam M, Rafii-Tabar H (2009) Comment on " Band structure engineering of graphene by strain: First - principles calculations". Phys Rev B 80: 167401-167403.
72. Mohiuddin TMG, Lombarto A, Nair RR, Bonetti A, Savini G, et al. (2009) Uniaxial strain in graphene by Raman spectroscopy: G peak splitting, Grűneisen parameter and sample orientation. Phys Rev B 79: 205433-205438.
73. Vandecasteele N, Lazzeri M, Mauri F (2009) Boosting electronic transport in carbon nanotube. Phys Rev Lett 102: 19680-196804.
74. Costa SD, Fantini C, Righi A, Bachmatiuk A, Mark HR, et al. (2011) Resonant Raman spectroscopy on enriched ^{13}C carbon nanotubes. Carbon 49: 4719-4723.
75. Rodriguez-Nieva JF, Saito R, Costa SD, Dresselhaus MS (2012) Effect of 13C doping on the optical phonon modes in graphene: Localization and Raman spectroscopy. Phys Rev B 85: 245406-245408.
76. Bernard S, Whiteway E, Yu V, Austing DG, Hilke M (2012) Probing the experimental phonon dispersion of graphene using ^{12}C and ^{13}C isotopes. Phys Rev B 86: 085409-085414.
77. Del Corro E, Kolbac M, Fantini C, M A Pimenta (2013) Isotopic $^{12}C/^{13}C$ effect on the resonant Raman spectrumof twiated bilayer graphene. Phys Rev B 88: 155436-155441.
78. Kun ZC, Yu LQ, Bo T, Huang Z, Lin W, et al. (2014) Isotope effect of the phonons mean free path in graphene by micro - Raman measurement, Science China. Phys Mech and Astro 57: 1817-1821.
79. Hass KC, Tamor MA, Anthony TR, Banholzer WF (1992) Lattice dynamics and Raman spectra of isotopically mixed diamons. Phys Rev B 45: 7171-7182.
80. Plekhanov VG (2020) Nonaccelerator study of the residual strong nuclear interaction. Intern J Theor and Comp Phys 1: 1-9.
81. Miller GA (2007) Charge density of the neutron. Phys Rev Lett 99: 112001-112005; Gloët IC, Miller G (2009) Neutron properties in the medium. Phys Rev 103: 082301-082305.
82. Ling Jun Wang (2018) Unification of gravitational and electromagnetic fields. Phys Essays 31: 81-88.
83. Stampfer Ch, Fringe S, Güttinger J, Francoise M, Christian V, et al. (2011) Transport in graphene nanostructures. Front Phys 6: 271-293.
84. Sasaki (2018) Massive Dirac Fermions Signal in Raman Spectrum of Graphene. Phys Rev B 97: 115413-115419.
85. Plekhanov VG (2023) Solid-State Manifestation of Quantum Chromodynamics. Hadronic Journal 46: 359-457.
86. Roberts CD (2015) Hadron physics and QCD: Just the basic facts. J Phys Conf Ser 630: 012051.
87. Deur A, Brodsky SJ, Teramond GF (2016) The QCD running coupling. Prog Part Nucl Phys 90: 1-74.
88. Roberts CD (2020) Empirical consequences of emergent mass. Symmetry 12: 1468-1506.
89. Compton AH (1919) The size and shape of the electron. Phys Rev 14: 247-259.
90. Landau LD (1969) About fundamental problems, in Selected Papers 2: 421-424.